Nanoscale

Accepted Manuscript

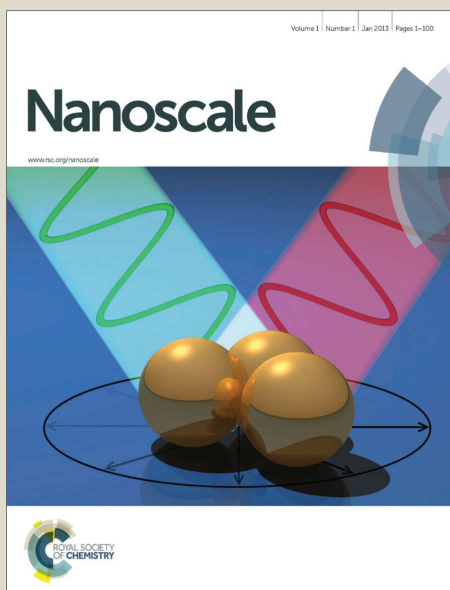

This is an *Accepted Manuscript*, which has been through the Royal Society of Chemistry peer review process and has been accepted for publication.

Accepted Manuscripts are published online shortly after acceptance, before technical editing, formatting and proof reading. Using this free service, authors can make their results available to the community, in citable form, before we publish the edited article. We will replace this *Accepted Manuscript* with the edited and formatted *Advance Article* as soon as it is available.

You can find more information about *Accepted Manuscripts* in the Information for Authors.

Please note that technical editing may introduce minor changes to the text and/or graphics, which may alter content. The journal's standard Terms & Conditions and the Ethical guidelines still apply. In no event shall the Royal Society of Chemistry be held responsible for any errors or omissions in this *Accepted Manuscript* or any consequences arising from the use of any information it contains.

ROYAL SOCIETY OF CHEMISTRY

www.rsc.org/nanoscale

Single Si nanowire (diameter ≤ 100nm) based polarization sensitive near-infrared photodetector with ultra-high responsivity

K. Das, S. Mukherjee, S. Manna, S. K. Ray and A .K .Raychaudhuri

Single silicon nanowire based MSM photodetectors show high responsivity (> 10^4 A/W) even at zero bias in near-infra-red region. The responsivity enhancement with reduced nanowire diameter has been explained by electric field enhancement shown by finite element based optical simulation. The observed photoresponse is sensitive to polarization of the exciting light, allowing the device to act as a polarization dependent photodetector.

Keyword: Si nanowires, photodetectors, high responsivity

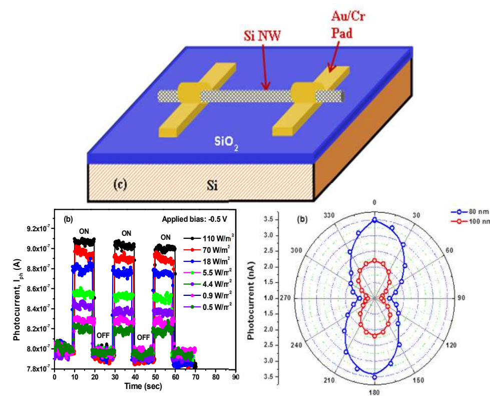

Nanoscale Accepted Manuscript

Journal Name RSCPublishing

ARTICLE

Single Si nanowire (diameter ≤ 100nm) based polarization sensitive near-infrared photodetector with ultra-high responsivity

Cite this: DOI: 10.1039/x0xx00000x

Received 00th January ****,
Accepted 00th January ****

DOI: 10.1039/x0xx00000x

www.rsc.org/

K. Das,[a] S. Mukherjee,[b] S. Manna,[c] S. K. Ray,[c,*] A .K .Raychaudhuri[a,#]

We report on the fabrication and optical response of boron doped single silicon nanowire based metal-semiconductor-metal photodetectors. Typical single nanowire devices were made from nanowires, grown by metal-assisted chemical etching process, with diameter ~80-100 nm and with electrode spacing ~1μm, using electron-beam lithography. A high responsivity of the order of 10^4 A/W has been observed even at zero bias in a single nanowire photodetector with peak responsivity in the near-infrared region. The responsivity has been found to be enhanced with increasing bias and reduced nanowire diameter. Finite element based optical simulation has been proposed to explain the diameter dependent performance of the single nanowire. The observed photoresponse is sensitive to the polarization of the exciting light source, allowing the device to act as a polarization dependent near-infrared photodetector.

A. Introduction

The observation of high photoresponsivity in semiconductor nanowires (NWs) and the realization of the photoconduction mechanism in nano-dimensional systems with a high surface to volume ratio has attracted growing curiosity for the potential use of NWs in integrated optoelectronic devices [1-3], hybrid organic–inorganic solar cells [4-6], optical interconnects [7-8], transceivers [9-10], etc. Silicon nanowires (NWs) are one of the most researched one-dimensional nanomaterials because of their compatibility with CMOS processing, controlled resistivity and high thermal conductivity. Si NWs have been used in wide range of prototype applications, such as solar cells [11-12], field effect transistors (FETs) [13-14], nanosensors [15-17], light emitting diodes (LEDs) [18-19], and photodetectors [20-22]. Significant efforts are being made on single nanowire based detector devices to achieve miniaturized devices with high responsivity, high gain and low noise with large bandwidth and short response time.

The growth of Si nanowire arrays over a large area with controlled diameter is a pre-requisite for the device application. Therefore the bottom-up approaches like vapor-liquid-solid (VLS) growth using molecular beam epitaxy (MBE), supercritical fluid liquid solid (SFLS), and laser ablation are more attractive than the conventional top-down ones employing nano-lithography methods and deep reactive ion etching (DRIE). However, recently the facile metal-assisted-chemical etching (MACE) method has been introduced to from Si NWs over a large area without sophisticated lithography technique [23-25].

Photodetectors fabricated with Si NW arrays and individual Si NW has shown rather low-responsivity in the near-IR region [26-27]. In this paper, we report the fabrication and opto-electronic characterization of single silicon nanowire metal-semiconductor-metal (MSM) photodetector devices exhibiting ultra-high responsivity in the near-IR region.

The responsivity is very high even without any external bias, making them attractive for low power devices. Also, the feasibility of fabrication of a photo-detector element of high responsivity with NW's of diameter ≤ 100nm opens up the possibility of high integration density devices for photonic applications. The observed variation of photocurrent as a function of the orientation of linear polarized light is reported for the single nanowire device, making it attractive for novel polarization-sensitive photodetectors.

B. Experimental

Arrays of Si NWs were fabricated by metal (Ag) assisted electroless chemical etching technique reported elsewhere [28-30]. The starting substrate was p-type, (100) oriented with a resistivity of 0.77 Ω-cm. The doping concentration of resulting NW, obtained after etching, is the same as that of the B-doped Si substrate (2 x $10^{16}/cm^3$). The typical length of NWs was ~30 μm and the diameter varied from 30–400 nm. A typical SEM image of a collection of as grown Si nanowires is shown in Fig. 1(a). Since the present investigation has been done on a single strand of a Si NW, we choose a wire with a specific diameter from the ensemble. Si nanowire suspension was dropped on oxidized Si substrates (SiO_2 thickness ~300nm) and Cr/Au contact electrodes were patterned on the selected single NW by the combination of photolithography and electron beam

Nanoscale Accepted Manuscript

This journal is © The Royal Society of Chemistry 2013

lithography. The e-beam lithography process was done using dual beam Helios 600 (FEI) system. The device fabrication was completed by thermal evaporation and lift-off process. The spectral photo-current response of the nanowires was measured using a set-up consisting of a calibrated broadband light source, a monochromator, a mechanical chopper (set to 180 Hz) and a lock-in amplifier (Stanford Research, SR 530). The device photocurrent was studied using a Keithley semiconductor parameter analyzer (Model no. 4200-SCS). The polarizer selectivity was measured using a polarizer.

C. Results & Discussions

We had fabricated several devices for similar diameter nanowires. In addition, multiple contact pads have been employed to verify the uniformity and reproducibility of our results for a single nanowire device. However, in the present paper, we show the results of two photodetector devices with different nanowire diameters and electrode spacings. The details of the device geometry and obtained results are summarized in table–I. The scanning electron microscopy image of device S-2 (wire dia. ~80 nm) is shown in Fig. 1(b), whereas the schematic diagram of the fabricated single NW photodetector device is shown in Fig.1(c).

The photoresponse of the nanowire devices was studied at a fixed illumination wavelength of 514 nm (Ar^+ laser) with varying applied bias and illumination power. The illumination source was pulsed using the mechanical chopper. Fig. 2(a) shows the typical pulsed photocurrent response of one of the nanowires (sample S-2). The data were taken with zero applied bias. The zero-bias dark current is very low of the order of ~0.4 nA. Upon illumination, in the example shown, the current rises to ~ 1.4 nA and it drops to the initial dark current value when the illumination is turned off. The currents in the states with illumination ON and OFF states remain the same within the noise level for consecutive cycles. From the optical modulation measurements, the nanowires device is found to exhibit fully reversible switching behavior, indicating the potential of the single Si NW device as an optical switch. It may kindly be noted that a significant photocurrent is generated even with zero bias. This is an important observation as this indicates that the separation of photo-generated electron–hole pairs can take place in the depletion region by an axial built-in electric field [31-33].

The photocurrent characteristics (for device S-2) measured with an applied bias of -0.5V for varying illumination intensity is shown in Fig. 2(b). The variation of photocurrent as a function of the incident power density (P) is shown in Fig. 3. Enhancement of the illumination intensity leads to enhanced electron-hole pair generation which enhances the device current. However, the photocurrent increases sub-linearly with excitation power. The sub-linear dependence of the photocurrent (I_{ph}) on illumination power (P) indicates that the mechanism of optical response is associated with carrier trapping. The experimental data have been fitted with a power law relation $I_{ph} \propto P^{\alpha}$. For both the devices the exponent α was found to be substantially lower than unity (~0.3), indicating existence of trap states in the nanowire with a broad range of energy. The exponent depends on the process of electron-hole generation, trapping, and recombination of the carriers within the nanowire [34]. The exponent $\alpha < 1$ has been observed in a number of photoconductors and it arises due to existence of localized traps near the band edges that controls the process of recombination and the resulting in photocurrent [34]. The energy distribution of the localized state around the Fermi level determines the value of α. If the localized states are distributed with an exponential dependence with the density of states near the conduction band edge (E_C), so that the density of states and the exponent can be expressed as [34]:

$$g(E) = g(E_C)e^{-\frac{(E_C-E)}{E^*}} \quad \text{................(1.a)}$$

and

$$\alpha \approx \frac{E^*}{E^* + k_B T} \quad \text{...............(1.b)}$$

where $g(E), g(E_C)$ are densities of states at energies E and E_c respectively. E^* is a characteristic energy scale. From the observed value of $\alpha \approx 0.3$, we find $E^* \approx 0.43$, $k_B T \approx 10$ meV at room temperature. This, however, is a small fraction of the value of the band gap for Si.

The band diagram of the nanowire device, for the zero bias and for an applied bias of V_R to one side is shown in Fig. 4(a) and 4(b), respectively. In metal-SiNW-metal photodetectors there are two dominant processes. One contribution to the photocurrent arises due to collection of generated carriers at the metal-nanowire Schottky contacts and the other contribution arises from the band bending caused by nanowire surface states. Both effects lead to increase in the photocurrent of the photodetector devices [35-37]. The increased carrier density (upon illumination) in Si NW would narrow the Schottky barrier width, which is equivalent to a lowering of the effective barrier height. The reduced barrier height at the contacts leads to enhancement of the device current

The performance of a photodetector is quantified in terms of the responsivity, which is directly related to the internal gain of the device. Responsivity (*R*), external quantum efficiency (EQE) and detectivity (D) are key parameters for a photodetector, which reflect the sensitivity of a photodetector to the incident light. To exclude the influence of the variation of the incident light power with wavelength on the photocurrent, responsivity (*R*) is a better physical quantity to be evaluated for obtaining the spectral response. The responsivity of a photodetector is defined as $R=J_{ph}/P$ where J_{ph} is the photocurrent density and P is power density of light source for a specific wavelength.

The spectral photoresponses of the Si NW MSM photodetectors have been characterized by measuring the responsivity in the spectral range from 400 to 1000 nm using a calibrated broad band source. The calibration was done by using a calibrated photodetector. The data for the two devices are shown in Fig. 5. Both the devices show broad spectral response varying from visible to near-IR range with a peak centered around 900 nm, which is associated with intrinsic transition above the band-edge of Si. The zero-bias peak responsivity *(R)* for device S-1 (~100 nm dia) is ~1.2 x 10^4 A/W while that for device S-2 (~80 nm dia) is ~2 x 10^4 A/W. Both the values are higher than the zero-bias responsivity reported till date, at room temperature for photodetectors fabricated with bulk or nanostructured Si [20-21,33,38]. The responsivity gets enhanced considerably with applied bias. For instance even a small applied bias of 0.1V enhances the responsivity by a factor

Nanoscale Accepted Manuscript

This journal is © The Royal Society of Chemistry 2012

of 2. With increase in applied reverse bias, the depletion region width increases. Therefore, the Schottky barrier devices generate larger number of photo-electrons and holes, which are easily swept out due to the lowering of barrier height, leading to the enhancement of gain. The highest responsivity reported so far for photodetectors with Si nanowire arrays is around 10^4 A/W in the range of 400-800 nm with a bias voltage of 1.0 V [39] at room temperature. It may be noted that the photodetector responsivity can get enhanced further on cooling to 150K or below, as reported before [26].

The enhancement of photoconductivity is quantitatively evaluated by evaluating the photoconductive gain (G), also known as the external quantum efficiency (EQE). The photoconductive gain is defined as the ratio of collected carriers per incident photon absorbed by the NW in a unit time ($G = N_{carrier}/N_{photon}$)

$$G = \frac{N_{carrier}}{N_{photon}} = \frac{(J_{ph}/e)}{P}\left(\frac{hc}{\lambda}\right) = R\frac{hc}{e\lambda} = R\frac{1240}{\lambda(nm)} \quad \ldots\ldots\ldots (2)$$

This gain G is related to the electronic transport and carrier collection efficiency during the photoconduction process. The physical meaning of G is related to the number of electrons circulating through the photoconductor per absorbed photon per unit time [40],

$$G = \frac{\tau}{t} = \frac{\tau}{l^2/D} = \frac{\tau\mu E}{l^2} \quad \ldots\ldots\ldots\ldots\ldots\ldots (3)$$

Where τ is the carrier life time, t is the transit time, l is the channel length of the photodetector, D is the diffusion coefficient and μ is the mobility of carriers. As discussed in equation (3), the gain of the photodetector is inversely proportional to square of the active length (electrode spacing) of the nanowire. For NW with the electrode separation comparable to the depletion width, there exists an axial field in the middle of the NW even in the absence of an applied bias. This leads to the higher carrier collection efficiency for shorter length nanowires. It may also be noted that the gain of the nanowire photodetector varies with the minority carrier parameters, D and μ in equation (3), which are strongly dependent on the dopant type and concentration. The calculated gain is found to very high and exceeds 10^5. The high photoconductive gain can be attributed to the combination of relatively long photocarrier life-time in Si compared to the short carrier transit time in the devices used because of the small spacing between the electrodes. It may be noted the electrode spacing of 100 nm and 80 nm diameters is 0.850 μm and 1.2 μm, respectively. It is clear from eqn. (3) that the responsivity value of the 80 nm nanowire is expected to be much higher, if the electrode spacing is normalized to that of 100 nm one.

Figure of merit of the photodetector has been determined by estimating the detectivity and the noise equivalent power (NEP), which is the minimum incident power that a detector can differentiate from the noise. The detectivity is related to the NEP by an equation as [29],

$$D = \frac{\sqrt{A.\Delta f}}{NEP} \quad \ldots\ldots\ldots\ldots\ldots\ldots\ldots (4)$$

where D is detectivity measured in cm $Hz^{1/2}$/W (or Jones), A is the effective detector area in cm^2, Δf is the electrical bandwidth in Hz. The detectivity is limited mainly by the three types of noise, namely, shot noise from dark current, Johnson noise and flicker noise from thermal fluctuation. We evaluated the noise current at zero bias taking into consideration both the shot noise as well as the Johnson noise since the resistance of the nanowire is known. The two noises namely the Jhonson noise as well as the thermal noise makes comparable contributions, but lower than that contributed by the shot noise. At zero bias the flicker noise contribution is zero. It may be noted that electrical noise has been measured in single Si nanowire recently, and the flicker noise was found to be rather low [41]. For estimation, we may thus consider that the shot noise (Noise power $=2qI_d$) is the dominant source of the noise. The spectral dependence of the detectivity, D(λ) can be estimated from the following equation [42],

$$D(\lambda) = \frac{R(\lambda)}{\sqrt{2qJ_d}} \quad \ldots\ldots\ldots\ldots\ldots\ldots (5)$$

where R is the responsivity, J_d is the dark current density and q is the electronic charge. The detectivity limit for our devices is tabulated in Table-I. The detectivity of 80 nm diameter nanowire is found to be higher as compared to that for 100 nm diameter wire. The responsivity and detectivity of the present single Si NW device are compared with those reported in the literature for different nanowire photodetectors and presented in Table-II.

The polarization selectivity of the single Si NW photodetector has been studied. It has been experimentally demonstrated that the NW optical excitation is most efficient under the incidence of linearly polarized light in the direction parallel to the NW axis [43]. Our devices also show polarization anisotropy with parallel excitation generating a higher photocurrent over that of perpendicular excitation, as shown in Fig 8(a), for device S-1 and S-2. The polar plot of the polarization dependent photocurrent is presented in Fig. 8(b).

D. Simulation

An important observation that we have made in the present investigation is the dependence of the responsivity on the diameter, in particular, the discernible enhancement of the responsivity when the diameter is reduced down to sub 100 nm region. We have carried out the simulation as described below in order to explain the above phenomena. The simulation shows that the enhancement in R occurs due to significant enhancement in the electric field of the incident light when the diameter decreases, particularly below 200 nm. We describe the simulation briefly below.

There exists an ultrathin (2-3 nm) SiO_2 layer on the Si NW (as detected by high resolution Transmission Electron Microscopy). The oxide serves as a passivation layer to reduce the dangling bonds on the NW surface. However, there is a significant difference of refractive index between the interior of nanowire, the surface SiO_2 and their surrounding ambience (air). The refractive index of Si is around n~3.65 corresponding to an input wavelength (λ=900 nm) [44], while it is 1.45 for SiO_2 and 1.0 for the surrounding material (air). Therefore, a steep difference of refractive index between the core (Si NW) and claddings (SiO_2 and air), results in large numerical aperture (NA), leading to the confinement of incident light and guiding through the wires. From the simulation, we demonstrate that the incident light can be waveguided into a nanowire causing the enhancement of quantum efficiency with reduced nanowire diameter. We have performed a two dimensional simulation with the finite element simulator COMSOL MULTIPHYSICS (4.3), using the RF MODULE. At the left edge, a plane wave is generated at a

Nanoscale Accepted Manuscript

port boundary condition. At the right edge of the NW is also a port boundary condition but without excitation to ensure the complete absorption of the incoming waves. A single Si NW of variable diameter and 5 um length, covered by the 2 nm oxide layer have been used in the simulation. The analytic solution is found by assuming that the electric field along the direction of propagation varies as,

$$E_Z = E_y e^{-ik_x . x} \quad \text{…………… (6.a)}$$

where, $E_y = C_1 \cos(k_y . y)$ inside the core ……. (6.b)

and, $E_y = C_0 e^{-[\eta|y| + r_{NW}]}$ outside the core ……. (6.c)

Because the electric fields must be continuous at the interface, the guidance condition must satisfy the following equations,

$$\eta = k_y \tan(k_y . r_{NW}) \text{ and } k_y^2 = k_{core}^2 - k_{cladding}^2 - \eta^2 \quad \text{…… (6.d)}$$

By solving these above equations, one can easily get the E_z value. The time averaged power loss (or equivalently, absorbance) can be determined by,

$$\Gamma_{avg}(\vec{r}) = \frac{1}{2} \Lambda |E_Z(\vec{r})|^2 \quad \text{……… (7)}$$

where, $\Lambda = \varepsilon . c$, where ε is the permittivity of the material and c is the velocity of light. In general, silicon has low absorption coefficient, but the photo-detection performance depends on the light trapping scheme, which controls the number of photo-generation carriers in Si photodetector. We propose that the existence of random pores in textured and electroless etched Si NWs, to enhance the absorption compared to planar Si surface due to multiple reflections.

The quantum efficiency (Q.E.) for monochromatic light is calculated by

$$Q.E.(\lambda) = \frac{\int \Gamma_{avg.}(\vec{r}) dr}{P_{avg.incident}} \quad \text{……… (8)}$$

where the average of the incident power $P_{avg\ incidnt}$ is the time-averaged Poynting vector of the monochromatic incident electromagnetic waves. In the above equation, it is assumed that the electrodes collect all the photo-generated electron-hole pairs which contribute to electrical current. As we know that, Q.E. is directly proportional with the responsivity of the photodetector, a higher Q.E. gives higher response. The optical simulation result shows the electric field energy distribution inside a single Si NW with varying diameter. The results in Fig. 6(a) and (b) show that the photon energy confined within the volume is significantly larger in the nanowire with smaller diameter. The estimated distribution of the electric field inside the nanowire (along the long axis) and at the SiO_2 cladding are shown in Fig. 7. As the diameter of the nanowire decreases, the electric field confinement within the Si core is enhanced rapidly. However, when the NW diameter is reduced below ~ 60 nm, a significant amount of electric field spreads into the cladding. This will result in the reduction of responsivity.

The simulation results also allow us to explain the observed polarization dependence of the response. If the incident electric field is polarized parallel to the axis of the nanowire, the amplitude of the electric field inside the nanowire will be same as the incident one in vacuum/air. But when the electric field is perpendicular to the nanowire axis, its amplitude inside the NW will be reduced by a factor depending on the material dielectric constant and its diameter [45].

Therefore, $$E_{in} = E_{exc} \quad \text{…….. (9.a)}$$

$$E_{in}^{\perp} = \frac{2\varepsilon_0}{\varepsilon_0 + \varepsilon} E_{exc} \quad \text{…….. (9.b)}$$

Where E_{exc} and E_{in} are the electric field amplitudes of the excitation and inside the cylindrical nanowire, respectively. ε_0 and ε are permittivity of the vacuum and the nanowire material. The polarization anisotropy is defined as,[45]

$$\sigma = \frac{I - I_{\perp}}{I + I_{\perp}} = \frac{1 - \left(\frac{2\varepsilon_0}{\varepsilon_0 + \varepsilon}\right)^2}{1 + \left(\frac{2\varepsilon_0}{\varepsilon_0 + \varepsilon}\right)^2} \quad \text{…………. (10)}$$

Where I and $I_{\perp}$ are the photocurrent due to the incident polarized light along the major and minor axes of the nanowire, respectively. The degree of linear polarization can be obtained from the photocurrent amplitude using equation (10) and the degree of anisotropy is estimated for three devices made with nanowires of different diameters. The result is shown in Fig. 9. It is found that the polarization anisotropy increases as the diameter is reduced. The results show that the single nanowire based devices can be extremely useful for polarization sensitive optical detection. The reason for the enhanced polarization anisotropy with reduced NW dimension is not clear at this moment.

Conclusions

In summary, we have demonstrated highly responsive metal-semiconductor-metal photodetectors fabricated with single Si nanowires which were prepared by a simple chemical-etching technique. The photo detectors show large zero bias photo response. The photodetector with 80 nm diameter NW exhibits maximum zero-bias peak responsivity of ~2.5×10^4 A/W in near infra-red wavelength (900 nm), which is much higher compared to those reported for Si nanowire based devices. Near complete depletion and collection of photogenerated carriers are achieved at a very low bias (-0.2 V), making the detector extremely attractive for low power operation. The device also exhibits good response and recovery to illumination and good reversibility between ON and OFF states. The single nanowire photodetectors have been found to exhibit high linear polarization selectivity. The responsivity as well as the polarization anisotropy is found to increase with the reduction of nanowire diameter. However, it appears that for NW of much smaller diameter the responsivity may become low. These results demonstrate the promising features of single Si NW devices for high gain, low power, polarization sensitive photodetection and optical switching in near IR region.

Acknowledgements

KD and AKR would like to acknowledge DST, Government of India for financial support as Theme Unit of Excellence in Nanodevice Technology. The partial support from DST "GPU" project at IIT Kharagpur is gratefully acknowledged. SM and SKR would like to acknowledge

Nanoscale Accepted Manuscript

 This journal is © The Royal Society of Chemistry 2012

Prof. Soumen Das, SMST, IIT Kharagpur for fruitful discussions. AKR acknowledges partial support from J.C.Bose Fellowship.

Notes and references

[a] Theme Unit of Excellence in Nanodevice Technology, S.N. Bose National Center for Basic Sciences, Sector-III, Salt Lake, Kolkata-700098, India.
[b] Advanced Technology Development Centre, Indian Institute of Technology, Kharagpur- 721302.
[c] Department of Physics, Indian Institute of Technology, Kharagpur-721302.
* physkr@phy.iitkgp.ernet.in
# arup@bose.res.in

1 Y. Xia, P. Yang, Y. Sun, Y. Wu, B. Mayers, B. Gates, Y. Yin, F. Kim and H. Yan, *Adv. Mater*., 2003, **15**, 353.

2 Y. Cui, Charles M. Lieber, *Science*, 2001, **291**, 851.

3 A. Zhang, S. You, C. Soci, Y. Liu, D. Wang, and Y-H. Lo, *Appl. Phys. Lett*., 2008, **93**, 121110.

4 F. Zhang, B. Sun, T. Song, X. Zhu, and S. Lee, *Chem. Mater.,* 2011, **23**, 2084.

5 P. Yu, C-Y. Tsai, J-K. Chang, C-C. Lai, P-H. Chen, Y-C. Lai, P-T. Tsai, M-C. Li, H-T. Pan, Y-Y. Huang, C-I Wu, Y-L. Chueh, Shih-Wei Chen, Chen-Hsun Du, Sheng-Fu Horng, and Hsin-Fei Meng, *ACS Nano*, 2013, **7**, 10780.

6 X. Shen, B. Sun, D. Liu, and S-T. Lee, *J. Am. Chem. Soc.*, 2011, **133**, 19408.

7 S. Pathak, D. V. Thourhout, and W. Bogaerts , *Optics Letters*, 2013, **38**, 2961.

8 K. Okamoto and K. Ishida, *Optics Letters*, 2013, **38**, 3530.

9 Xun Li, Gui-Rong Zhou, Ning-Ning Feng and Wei-Ping Huang, *IEEE Photon. Technol. Lett.*, 2005, **17**, 1214.

10 S. Bidnyk, D. Feng, A. Balakrishnan, M. Pearson, M. Gao, H. Liang, W. Qian, C. C. Kung, J. Fong, J. Yin, and M. Asghari, *IEEE Photon. Technol. Lett.*, 2006, **18**, 2392.

11 B Tian, X Zheng, TJ Kempa, Y Fang, N Yu, G Yu, J Huang, CM Lieber, *Nature,* 2007, **449**, 885.

12 L. Hu and G. Chen, *Nano Lett.*, 2007, **7**, 3249.

13 Y Cui, Z Zhong, D Wang, W U. Wang, and C M. Lieber, *Nano Lett.*, 2003, **3**, 149.

14 X. Duan, Y. Huang, Y. Cui, J. Wang & C M. Lieber, *Nature*, 2001, **409**, 66.

15 J. H. Chua , R-E. Chee , A. Agarwal , S. M. Wong and G-J. Zhang, *Anal. Chem.*, 2009, **81,** 6266.

16 F. Patolsky, G. Zheng & C. M Lieber, *Nature Protocols*, 2006, **1**, 1711.

17 G. Zheng, F. Patolsky, Y. Cui, W. U Wang & C. M Lieber, *Nature Biotechnol.*, 2005, **23**, 1294.

18 F. Qian, S. Gradecak, Y. Li, C-Y. Wen, and C. M. Lieber, *Nano Lett.*, 2005, **5**, 2287.

19 O. Hayden, A. B. Greytak and D. C. Bell, *Adv. Mater.*, 2005, **17**, 701

20 M. Ahmad, K. Rasool, M. A. Rafiq and M. M. Hasan, *Appl. Phys. Lett.,* 2012, **101**, 223103.

21 E. Mulazimoglu, S. Coskun, M. Gunoven, B. Butun, E. Ozbay, R. Turan and H E. Unalan, *Appl. Phys. Lett.*, 2013, **103**, 083114.

22 S-J. Choi, Y-C. Lee, M-L. Seol, J-H. Ahn, S. Kim, D-I Moon, J-W.Han, S. Mann, J-W. Yang and Y-K.Choi, *Adv. Mater*., 2011, **23**, 3979.

23 C. Yang , C. J. Barrelet, F. Capasso, and C. M. Lieber, *Nano Lett.,* 2006, **6**, 2929.

24 X. Li and P. W. Bohn, *Appl. Phys. Lett*., 2000, **77**, 2572.

25 C-Y. Chen, C-S. Wu, C-J. Chou and T-J. Yen, *Adv. Mater*., 2008, **20**, 3811.

26 A. Zhang, H. Kim, J. Cheng and Y-H. Lo, *Nano Lett.*, 2010**, 10**, 2117.

27 L.B. Luo, L.H. Zeng, C. Xie, Y.Q. Yu, F.X. Liang, C.Y. Wu, L. Wang and J.G. Hu, *Sci. Rep*., 2014, **4**, 3914.

28 B. Ozdemir, M. Kulakci, R. Turan and H. E. Unalan, *Nanotech.* 2011, **22**, 155606.

29 S. Manna, S. Das, S. P. Mondal, R. Singha, and S. K. Ray, *J. Phys. Chem. C*, 2012**, 116,** 7126.

30 G. Fan, H. Zhu, K. Wang, J. Wei, X. Li, Q. Shu, N. Guo and D. Wu, *ACS appl. Mater. Interfaces*, 2011, **3**, 721.

31 Y. Ahn, J. Dunning and J. Park, *Nano Lett.*, 2005, **5**, 1367.

32 Y. Yang, W. Guo, J. Qi, J. Zhao, Y. Zhang, *Appl. Phys. Lett.*, 2010, **97**, 223113.

33 J. Bae, H. Kim, X-M. Zhang, C. H Dang, Y. Zhang, Y. J. Choi, A. Nurmikko and Z. L. Wang, *Nanotech.,* 2010, **21**, 095502.

34 A. Rose, "Concepts in Photoconductivity and Allied Problems", *Krieger Publishing Company*, New York, 1978.

35 H. Wang, *Appl. Phys. Lett.,* 2013, **103**, 093101.

Nanoscale Accepted Manuscript

36 K. D. Hof, C. Rossler, S. Manus, J. P. Kotthaus, A. W. Holleitner, D. Schuh, and W. Wegscheider, *Phys. Rev. B*, 2008, **78**, 115325.

37 R. Basori, K. Das, P. Kumar, K. S. Narayan and A. K. Raychaudhuri, *Appl. Phys. Lett.*, 2013, **102**, 061111.

38 S.O. Kasap, "Optoelectronics & Photonics: Principles & Practices", *Prentice Hall,* 2012.

39 S. Lee, S. W. Jung, S. Park, J. Ahn, S. J. Hong, H. J. Yoo, M. H. Lee, and D. -I. Cho, *MEMS 2012*, Paris, FRANCE, 29 January - 2 February 2012, **1364**.

40 R-S. Chen, T-H. Yang, H-Y. Chen, L-C. Chen, K-H. Chen, Y-J. Yang, C-H. Su and C-R. Lin, *Appl. Phys. Lett*., 2009, **95**, 162112.

41 S. Samanta, K. Das and A. K. Raychaudhuri, *Nanoscale Research Letters*, 2013, **8**, 165.

42 Z. Liu, T. Luo, B. Liang, G. Chen, G. Yu, X. Xie, D. Chen and G. Shen, *Nano Research*, 2013, **6**, 775.

43 M. H. M. van Weert, N. Akopian, F. Kelkensberg, U. Perinetti, M. P. van Kouwen, J. G. Rivas, M. T. Borgström, R. E. Algra, M. A. Verheijen, E. P. A. M. Bakkers, L. P. Kouwenhoven and V. Zwiller, *Small*, 2009, **5**, 2134

44 "Handbook of Optical Constants of Solids", Edward D. Palik. *Academic Press*, Boston, 1985.

45 J. Wang, M. S. Gudiksen, X. Duan, Yi Cui, C. M. Lieber, *Science*, 2001, **293**, 1455.

46 X. Dai, S. Zhang, Z. Wang, G. Adamo, H. Liu, Y. Huang, C. Couteau and C. Soci, *Nano Lett*., 2014, **14**, 2688.

47 S. L. Wu, T. Zhang, R. T. Zheng, and G. Cheng, *Chemical Physics Letters,* 2012, **538**, 102.

48 R. Zou, Z. Zhang, J. Hu, L. Sang, Y. Koide and M. Liao, *Nanotechnology*, 2013, **24**, 495701.

Nanoscale Accepted Manuscript

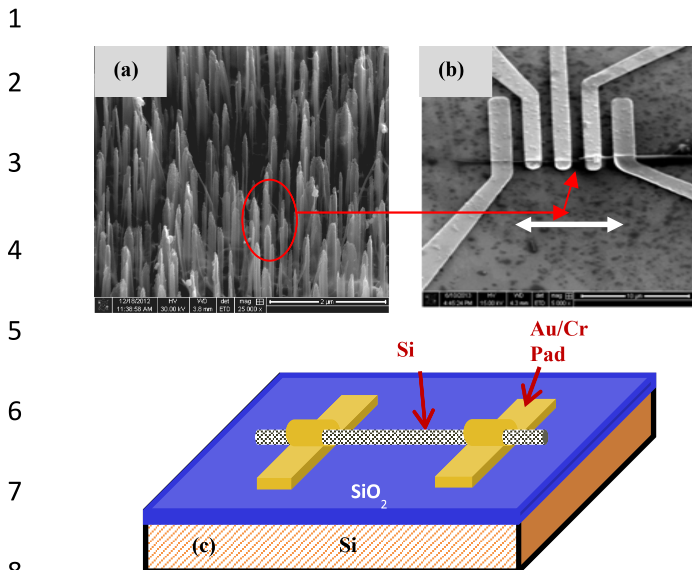

Figure 1 : SEM images of (a) bunch of as-synthesized silicon nanowires, (b) patterned metal electrodes on a single nanowire of diameter ~ 80 nm and (c) Schematic diagram of the fabricated single nanowire device.

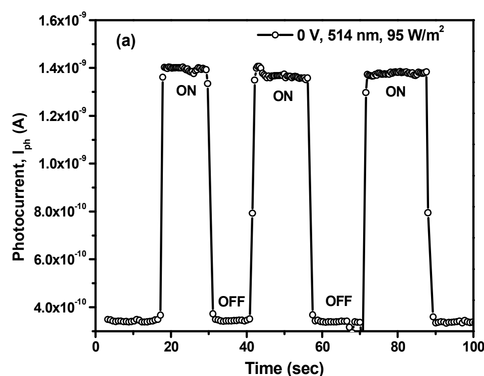

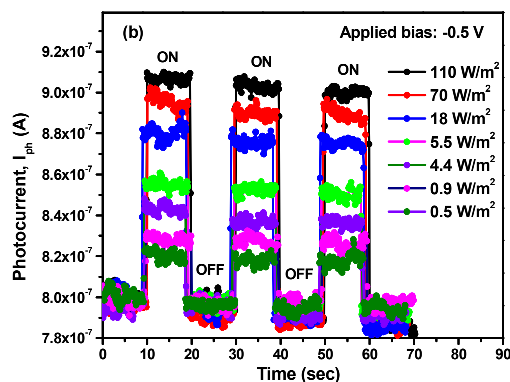

Figure 2: Optical modulation characteristics of single nanowire device S-2, (a) at zero bias for a fixed illumination power density (b) at a bias of -0.5 V with different illumination power density.

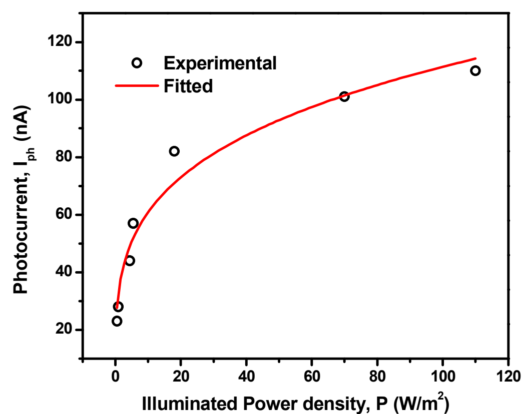

Figure 3: Variation of photocurrent as a function of the illuminated power density for single nanowire device, S-2.

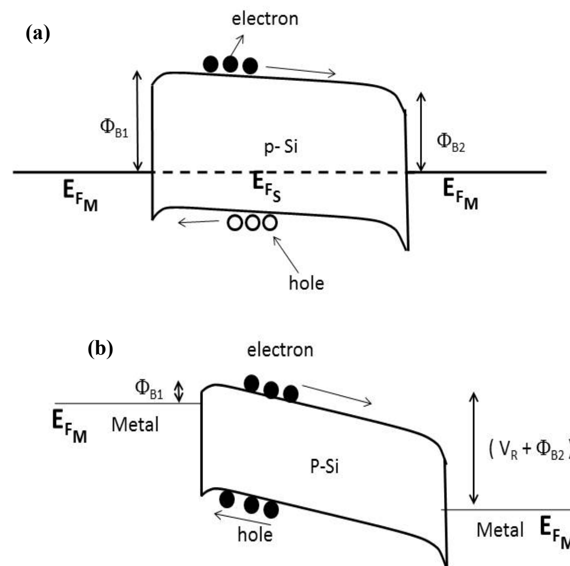

Figure 4: Band diagram of MSM photodetector device for (a) Zero bias and (b) near the flat-band condition for an applied bias, V_R to an electrode.

Nanoscale Accepted Manuscript

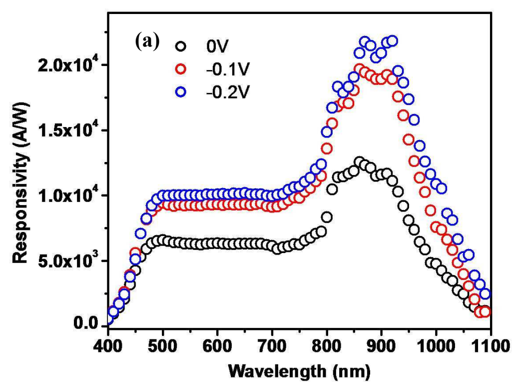

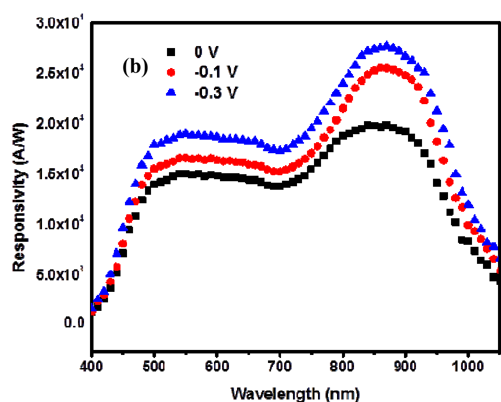

Figure 5: Spectral responsivity of single nanowire photodetector devices of (a) 100 nm dia and (b) 80 nm dia, for different applied biases.

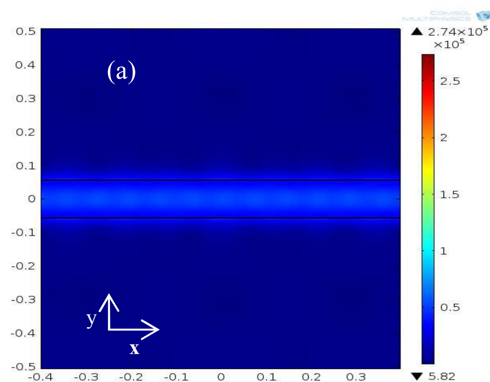

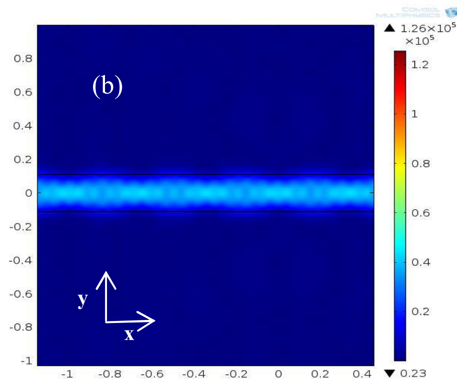

Figure 6: Electric field energy distribution inside a Si NW core surrounded by SiO2 cladding for diameter of (a) 100 nm and (b) 200 nm

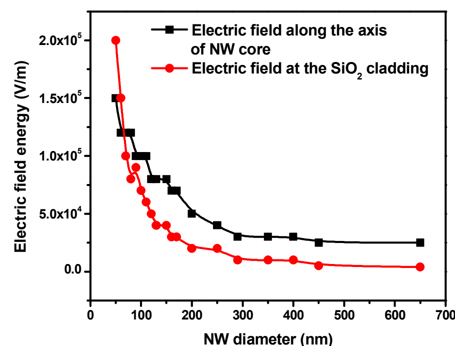

Figure 7: Electric field energy variation along the long axis of Si nanowire and at the interface, as a function of it's diameter.

Nanoscale Accepted Manuscript

This journal is © The Royal Society of Chemistry 2012

1
2
3
4
5
6

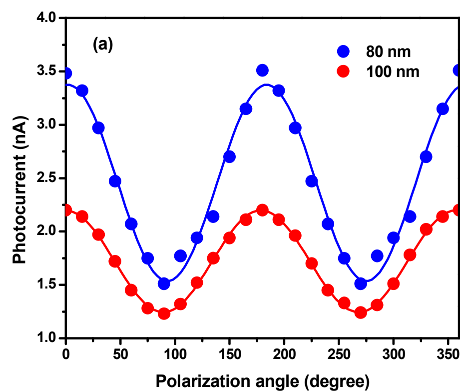

7
8
9
10
11
12

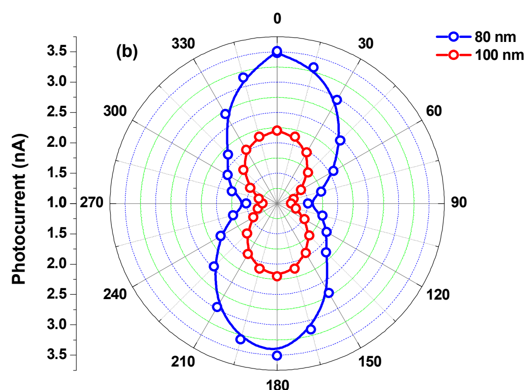

13
14 **Figure 8.** (a) Polarization angle dependent photocurrent for 80
15 nm and 100 nm nanowires, and (b) the polar plot of the
16 photocurrent for both the devices.

17
18
19
20
21
22

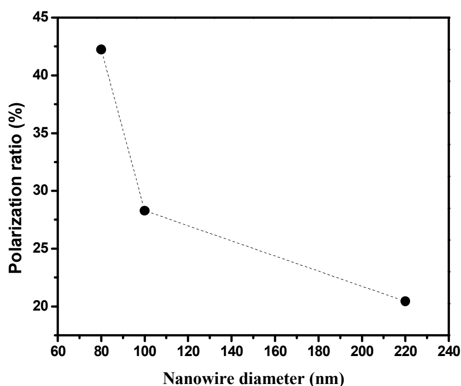

23 **Figure 9**: The variation of the polarization ratio as a function of
24 nanowire diameter. The dotted line has been drawn to guide the
25 eye.

26

27
28
29
30 **Table 1.** The details of the device geometry and obtained results
31

Device	Wire diameter (nm)	Electrode spacing (μm)	Responsivity (A/W) at a bias		Detectivity ($cmHz^{½}/W$)
			0 V	0.1 V	0 V
S-1	100	0.85	1.21 x 10^4	1.76 x 10^4	0.8 x 10^{13}
S-2	80	1.2	1.97 x 10^4	2.56 x 10^4	1.4 x 10^{13}

32
33
34
35
36
37
38
39
40
41
42
43
44
45
46
47
48
49
50
51
52
53
54
55

Nanoscale Accepted Manuscript

1

2 **Table-II:** Comparison of performance of nanowire based
3 photodetectors.

Device	Responsivity (A/W)	Detectivity ($cmHz^{½}/W$)	References
Single Si NW (80 nm)	1.97 x 10^4 (0 V) 2.56 x 10^4 (0.1 V)	~10^{13}	Present work
Ensemble (collection) of Si NWs (30-400 nm)	0.59 (1 V)	1.55 x 10^{10}	Ahmad et al. *Appl. Phys. Lett.*, 2012, **101**, 223103. [20]
Single core−shell GaAs/AlGaAs NW (40/170 nm)	0.57 (1 V)	7.2 × 10^{10}	Dai et al. *Nano Lett*. 2014, **14**, 2688. [46]
Ensemble (collection) of Si NWs (~200 nm)	0.6 (0.5 V)	-	Bae et al. *Nanotech.*, 2010, **21** 095502. [33]
Ensemble (collection) of Si NWs (100 nm)	0.58 (0.2 V)	-	Wu et al. *Chemical Physics Letters*, 2012, **538**, 102. [47]
Single InAs NW (138 nm)	4.4 x 10^3 (2 V)	2.6 x 10^{11}	Liu et al. *Nano Research*, 2013, **6**, 775. [42]
Single Ga_2O_3 NW (500 nm)	4.5 x 10^3 (10 V)	1.26 x 10^{16}	Zou et al. *Nanotech*., 2013, **24,** 495701. [48]
Ensemble (collection) of p-Si/n-CdS core-shell NW (~130 nm core with 65 nm shell)	1.37 (1.0 V)	4.39 × 10^{11}	Manna et al. *J. Phys. Chem. C*, 2012, **116**, 7126. [29]

4

Nanoscale Accepted Manuscript

 This journal is © The Royal Society of Chemistry 2012